MNPs@QDs

Subjects: Materials Science, Composites

Contributor: Haiyang Jiang , Jincheng Xiong , , Jiyue Cao

The presence of food contaminants can cause foodborne illnesses, posing a severe threat to human health. Therefore, a rapid, sensitive, and convenient method for monitoring food contaminants is eagerly needed. The complex matrix interferences of food samples and poor performance of existing sensing probes bring significant challenges to improving detection performances. Nanocomposites with multifunctional features provide a solution to these problems. The combination of the superior characteristics of magnetic nanoparticles (MNPs) and quantum dots (QDs) to fabricate magnetic fluorescent quantum dots (MNPs@QDs) nanocomposites are regarded as an ideal multifunctional probe for food contaminants analysis.

MNPs@QDs

1. Introduction

Currently, the preparation methods of MNPs@QDs have been reported with numerous literature [1][2]. The key points to consider in the reasonable integration of MNPs and QDs into multifunctional MNPs@QDs nanocomposites is whether the two components are firmly combined, and interact without causing loss of magnetic and fluorescent performance. Furthermore, its properties such as dispersibility, stability, biocompatibility and desirable surface functionalization are also related to its practical applications. Although the compositions and morphologies of these nanocomposites perform differently, most strategies can be divided into five categories: heterocrystalline growth, template embedding, LBL assembly, microemulsion technique and one-pot method.

2. Hetero-Crystalline Growth

Hetero-crystalline growth usually combines MNPs and QDs in either core-shell or two asymmetric nanoparticles (heterodimers). The deposition of semiconductor materials on the prefabricated magnetic nanocrystals by decomposing the precursors at high temperatures generate the formation of MNPs@QDs nanocomposites with distinct functional domains. The typical core-shell structures were reported such as Co@CdSe [3], Fe_3O_4/CdSe/ZnS [4][5], and Fe_3O_4@PANI/CQDs [6]; and heterodimer structures such as FePt-Pb (S, Se) [7], FePt@CdS [8], Fe_2O_3-CdSe [9][10], Fe_3O_4-CdS (Se) [11][12]. Gu et al. reported a simple synthesis route for producing heterodimer nanoparticles by employing lattice mismatching and high-temperature decomposition [8]. In the presence of oleylamine and oleic acid, Fe@Pt was firstly formed at high-temperature decomposition. Subsequently, S and Cd were successively deposited on the surface of Fe@Pt to form metastable core-shell nanostructures at 100 °C. With the increase of solution temperature to 280 °C, the amorphous CdS on the sphere's surface was transformed into a crystal and formed heterodimers FePt@CdS nanoparticles with an appropriate size

of 7 nm and a QY of 3.2% (**Figure 1**a) The core-shell or heterodimer MNPs@QDs all strongly depend on the lattice mismatch between the MNPs and QDs components, and synthesis conditions such as the reaction temperature, surface capping agents and the addition order of the precursors [7][8].

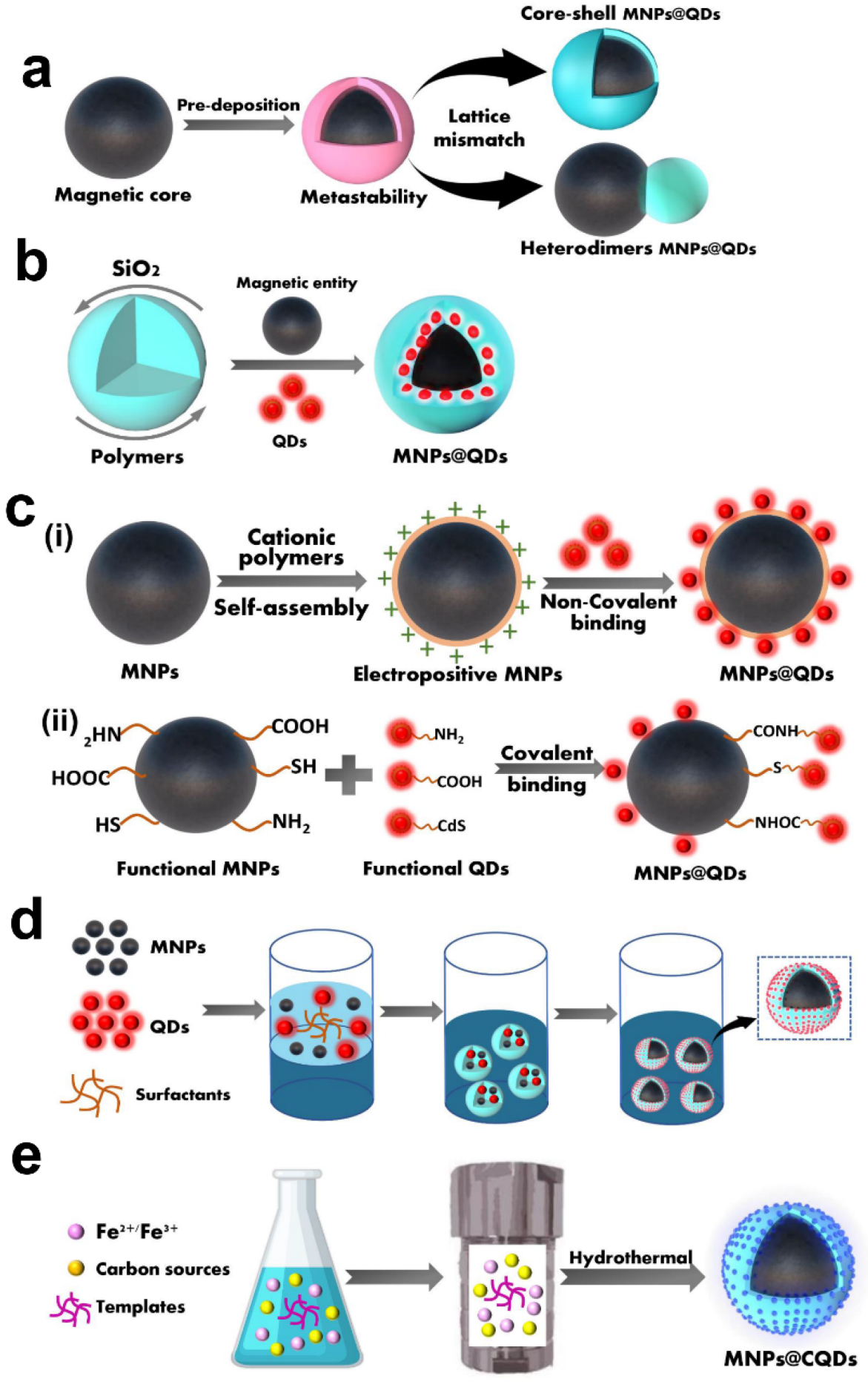
a
Core-shell MNPs@QDs
Pre-deposition
Lattice mismatch
Magnetic core
Metastability
Heterodimers MNPs@QDs
b
SiO2
Magnetic entity
Polymers
QDs
MNPs@QDs
c
(i)
Cationic polymers
Self-assembly
Non-Covalent binding
MNPs
Electropositive MNPs
MNPs@QDs
(ii)
2HN
COOH
HOOC
SH
HS
NH2
NH2
COOH
CdS
Covalent binding
CONH
S
NHOC
Functional MNPs
Functional QDs
MNPs@QDs
d
MNPs
QDs
Surfactants
e
Fe2+/Fe3+
Carbon sources
Templates
Hydrothermal
MNPs@CQDs

Figure 1. Schematic diagram of five preparation methods of MNPs@QDs nanocomposites. (**a**) Hetero-crystalline growth; (**b**) Template embedding; (**c**) Layer-by-layer assembly constitute of (**i**) non-covalent binding and (**ii**) covalent binding; (**d**) Microemulsion technique; (**e**) One-pot method.

Although the hetero-crystalline growth method was first reported for preparing MNP@QDs, the main problems of the method are the inability to optimize the properties of the nanocomposites, undesirable magnetic responsiveness, low QY, and lack of functional groups, which make it challenging to satisfy the diversified requirements of food contaminants analysis. The initial nanocrystals can be prepared under optimal conditions; however, in the preparation of subsequent components, the initial crystals may be subject to a series of temperature variations that affect their structure. Moreover, the undesirable interfacial interaction between MNPs and QDs may cause the loss of the dual performances of MNPs@QDs. The inner filter effect (IFE) (non-radioactive quenching) induced by MNPs and the poor crystal quality of QDs lead to the QY of MNPs@QDs usually less than 10%. For example, after passivating the surface layer of Fe_3O_4@CdSe by ZnS, the QY was increased from 2–3% to 10–15% [13]. This value was still much lower than that of standard CdSe/ZnS QDs alone [14]. The magnetism of MNPs is relatively easy to maintain, but interfacial doping or instability between two lattices may result in disorder in MNPs structure [15]; it is still a troublesome problem in the currently reported research by hetero-crystalline growth method.

3. Template Embedding

Template embedding usually encapsulates the discrete preformed MNPs and QDs into the liposomes [16], micelles [17][18], silica [19][20][21][22][23][24][25], and polymer materials [26][27][28][29][30] simultaneously to obtain MNPs@QDs. The spatial separation between MNPs and QDs helps avoid the mutual interference between the two components, reducing the possibility of reduced magnetic responsiveness or fluorescence quenching.

Silica (SiO_2) has the advantages of good biological inertia and biocompatibility, facile synthesis, and operable surface functionalization, which offer a favorable carrier for loading MNPs and QDs to form MNPs@QDs nanocomposites. Dong et al. encapsulated both Fe_2O_3 and CdSe QDs within a silica shell to form SiO_2/MNPs-QDs. The QY decreased appropriately 4- and 10-fold lower than bare CdSe QDs (QY = 11.4%) at the coating reacting at 8 and 48 h, respectively [22]. The quenching effect of MNPs and multiple chemical reactions still inevitably affects the dual performance of nanocomposites, and seeking better spatial separation is significant for its further application. The silica layer wraps on the surface of the MNPs as a classical strategy to construct an efficient barrier to prevent fluorescence quenching by adjusting the thickness of the silica shell. Easy manipulation of surface functionalization provides plenty of binding sites for QDs and recognition elements conjugation. Furthermore, the silica coating helps to reduce the toxicity of bare MNPs, and improve their stability and dispersity, which is conducive to subsequent biological applications [24][31][32][33]. Meanwhile, the hollow and mesoporous silica templates can effectively reduce the density of the silica, enhance the transmissivity of irradiation light, and avoid the side effects of absorption and scattering [19][20][25][34]. The general strategy of template embedment is illustrated in **Figure 1**b.

In addition to SiO_2, polymer materials are also employed as carriers for encapsulating MNPs and QDs, which is commonly achieved by hydrophobic [27][28][35], electrostatic [36], and covalent [37][38] interactions to encapsulate the two components into polymer materials. For example, Xie et al. used poly(styrene/acrylamide) copolymer nanospheres to embed MNPs and QDs, the hydrophilic groups of the copolymer were inclined to locate on the outer surface of nanospheres. At the same time, numerous hydrophobic moieties were found in the interior, leading to the formation of hydrophobic cavities [27]. Both hydrophobic CdSe/ZnS QDs (3–6 nm) and Fe_2O_3 (5–20 nm) can be directly embedded into the mesoporous to form multimodal hybrid nanocomposites. The common polymer materials used in these studies include poly(styrene/acrylamide) copolymer nanospheres [27][35], poly(styrene-co-ethylene glycol dimethacrylate-co-methacrylic acid) beads [28], poly(lactic-co-glycolic acid) (PLGA) [39], poly(glycidyl methacrylate) [40], poly(lactide)tocopherol polyethylene glycol succinate [26], and chitosan-based polyelectrolyte complexes [30][41].

Template-based embedding techniques utilize biocompatible materials to adjust the performance of the obtained nanocomposites, intending to improve their stability and dispersibility, modify functional groups, and reduce toxicity. The carrier of a huge interior cavity provides opportunities for high payloads of dual components and easy manipulation of desirable properties by changing the proportion of different types of components. High loading with MNPs could enhance magnetic responsiveness intensity and separation speed under an external magnetic field, thereby minimizing the separation time in complicated food matrices. Moreover, the different emission QDs could be embedded into SiO_2, enabling optical encoding of multiple food contaminants. The template embedding method to fabricate MNPs@QDs nanocomposites provides an ideal strategy for designing matrix tolerance and high-performance sensing probes.

4. Layer-by-Layer Assembly

LBL assembly integrates performed MNPs and QDs through non-covalent forces and chemical covalent bonds to form MNPs@QDs with a multi-layer self-assembled core-shell structure. The non-covalent interactions mainly involve electrostatic adsorption [42][43][44], hydrophobic [45], coordination [46], and biomolecule-assisted system [47][48]. The polyelectrolyte cationic polymers-mediated electrostatic adsorption is commonly used for preparing core-shell MNPs@QDs, such as the poly (allylamine hydrochloride)[42], poly (dimethyl diallyl ammonium chloride) [49], and polyethyleneimine (PEI) [43]. The negatively charged QDs were wrapped on the surface of positively charged PEI capped MNPs, while the luminescent intensity could be tuned by controlling the number of PEI layers to absorb different amounts of QDs [43][50][51] (**Figure 1**c). The amphiphilic poly(4-vinylpyrollidone) capped Fe_3O_4 nanoparticles can bind 1-dodecanethiol modified QDs via hydrophobic-hydrophobic interactions to form MNPs@QDs [45]. Alternatively, barnase-capped MNPs were tightly conjugated with barstar-capped QDs to form dual-functional MNPs@QDs via this protein-assisted noncovalent binding system [47], and the biotin-functionalized Fe_3O_4 conjugated with streptavidin-functionalized CdSe/ZnS QDs via the high-affinity streptavidin-biotin system [48]. The non-covalent interactions do not depend on complicated chemical reagents and synthesis, which provides a simple way to construct dual-functional MNPs@QDs nanocomposites. It is worth noting that the QDs may leak or drop from the linker-connected MNPs under certain conditions, which may affect the stability of the storage,

coupling, and practical applications. Moreover, the emission intensity is inevitably affected by MNPs to reduce the PL QY, which may be attributed to non-radiative energy or charge transfer processes during the assembly.

Another approach for LBL assembly is based on covalent binding between MNPs and QDs. The strategy utilizes reactive functional groups such as carboxyl (-COOH), amino (-NH_2), thiol, and siloxane groups to realize the connection of two components [52][53][54][55][56] (**Figure 1**c(ii)). NH_2-Fe_3O_4@SiO_2 is the most commonly used for coupling with COOH-QDs via the carbodiimide chemistry method [57][58]. Fe_3O_4 is easily modified with amino groups by the silanization treatment, and SiO_2 wrapped on the surface of Fe_3O_4 minimized the quenching effect and provided functional groups for enabling chemical bonding with QDs while solving the problems of easy aggregation and increasing their stability. The l-cysteine-modified ZnS QDs with rich amino are also applied for coupling with COOH-functionalized Fe_3O_4 to form MNPs@QDs, but the coupling efficiency may be reduced when recognition elements were used directly conjugating with the outer layer of amino-QDs [53]. The thiol modified Fe_3O_4@SiO_2 was used for binding QDs seeds on the surface. The carboxylic groups of the thiol ligands improved the water dispersity and surface functionality for further conjugation of bioactive molecules [59]. The 3-mercaptopropyltrimethoxysilane (APTES) capped ZnS QDs have trimethoxysilane groups, which can be easily connected via Si-O-Si bonds to create a SiO_2 network and conglutinated together with Fe_3O_4@SiO_2 in a nanosphere [55]. The covalent interaction provides a solid combination compared with non-covalent interactions. This approach increases the stability of nanocomposites and reduces the possibility of QDs leaking from the surface of the MNPs. The abundant functional groups of the dual components build a robust bridge for the construction of MNPs@QDs nanocomposites, and these active functional groups also provide diverse sites for the conjugation of specific recognition elements for convenient detection of multiple food contaminants. The LBL strategy to prepare MNPs@QDs nanocomposites has become popular due to its high simplicity, operability, and adaptability, satisfying the requirements of constructing rapid, sensitive multifunctional sensors for food contaminants analysis.

5. Microemulsion Technique

The microemulsion technique is a transparent or translucent, isotropic, thermodynamically stable system formed by water, organic solvents, MNPs, QDs, and surfactants in appropriate proportions. Chen et al. mixed hydrophobic QDs and MNPs with dodecyltrimethylammonium bromide (DTAB) to form an aqueous solution, and the mixture was then quickly poured into a poly(vinylpyrrolidone) (PVP) ethylene glycol (EG) solution. The obtained nanoparticles were 120 nm with a close-packed structure, MNPs preferentially became a magnetic core, QDs formed a fluorescent shell, and dipole-dipole interactions of MNPs and oleophobic interactions generated between MNPs and QDs promoted the structure formation [60]. A sol-gel process was introduced to encapsulate a thin silica shell on the surface of MNPs@QDs for improving biocompatibility and colloidal stability, and the obtained nanocomposites were successfully applied as a live cell tracer and dual-modal imaging probe [61].

Polymer beads for incorporating MNPs and QDs also attract considerable attention due to their simplicity and diversity. Guo et al. used trichloromethane containing octadecylamine-coated QDs (OC-QDs), oleic acid-modified MNPs (OA-MNPs), poly (methyl methacrylate) (PMMA), and poly (maleic anhydride-alt-1-octadecene) (PMAO)

composites to form MNPs@QDs through an ultrasonic emulsification solvent evaporation process [62]. The fluorescence intensity was 226 times that of corresponding QDs, and saturation magnetization still retained 45.4% of the compared MNPs. The ultrasonic emulsification introduced herein could conveniently control the size of nanocomposites, rendering them more suitable for point of care testing applications. The amphiphilic (2-hydroxyl-3-dodecanoxyl) propylcarboxymethyl chitosan [63], PLGA [64], poly (styrene-co-maleic anhydride) [65] also act as carriers, in which MNPs and QDs dissolved in the organic phase are transferred into the aqueous phase through hydrophobic interaction. The general strategy of template embedment is depicted in **Figure 1**d. The reaction process involves using more organic solvents or surfactants, and incomplete evaporation and washing to remove these reagents may damage the dual properties of MNPs@QDs. Moreover, the materials yield via this method is low, which is not conducive to its wide applications in food contaminants' rapid detection.

The microfluidic devices are also employed to simplify the process of producing standardized MNPs@QDs with uniform size and a controllable number of QDs within each particle. As depicted by Lan et al., the Fe_3O_4 and CdSe/ZnS QDs were respectively dispersed in the alginate solution within the corresponding inlet, and then co-flow was formed in the flow-focusing-channel [66]. Under the flow-focusing orifice, the Ca^{2+} in the oil phase was mixed with droplets, and many Janus droplets were produced by symmetric shearing, and droplets were solidified in the extension serpentine channel and collected at the outlet. The sodium alginate used herein provided an excellent carrier for cross-linked with Ca^{2+} to form a gel structure, and the COOH of the surface could be used for further biofunctionalization. Interestingly, Fe_3O_4 and QDs stayed in their respective hemispheres within a fairly symmetrical structure, which minimized the fluorescence quenching effect of MNPs and prevented the leakage of QDs. The microfluidic technology as a simple, convenient, and straightforward approach for producing MNPs@QDs with fantastic fluorescence and magnetism is of great potential, the dual properties of nanocomposites could be easily manipulated by adjusting the flow rate of liquid. The microfluidic-based microemulsion technique points the way for the production of standardized MNPs@QDs.

6. One-Pot Method

The one-pot method is to mix the precursors of MNPs and QDs in a vessel to complete the fabrication of MNPs@QDs in a single step. The hydrothermal method is a bottom-up strategy under high temperature and pressure and is frequently used for preparing MNPs@QDs nanocomposites in one step; their scheme illustration is presented in **Figure 1**e. In one study, Zhou et al. utilized graphite oxide (GO), cadmium chloride, ferric dichloride tetrahydrate, and sodium acetate as precursors and dispersed them in a DMSO solution to form a stable suspension. The mixture was then transferred into a Teflon-lined autoclave for a high-temperature reaction (180 °C for 12 h) to obtain nanocomposites [67]. The individual components were well distributed with no mutual interference. The high specific surface area and abundant negative charge of GO provided more nucleation sites for loading MNPs and QDs. The assembled nanocomposites exhibited favorable magnetism intensity (44.85 emu/g) and high loading efficiency (0.98 mg/mg) for doxorubicin.

In addition to QDs, carbon quantum dots (CQDs) were also employed to fabricate MNPs@QDs nanocomposites. There are two apparent merits of CQDs to prepare nanocomposites: (i) the inherent advantages of CQDs, such as

low cost, low toxicity, high surface area, abundant surface groups, favorable optical properties; (ii) the electrostatic repulsion generated by CQDs, which provides excellent colloidal stability for Fe_3O_4. Maleki et al. added $FeCl_3{\cdot}6H_2O$, ethylenediamine, and citric acid into deionized water and poured it into a Teflon-lined autoclave for heating at 200 °C for 5 h, the MNPs@QDs was synthesized, and its magnetism intensity reached 62.0 emu/g [68]. The CQDs derived from a onefold carbon source suffer a low QY, and heteroatom doping plays a crucial role in regulating the fluorescent intensity of CQD. Nitrogen-doping (N-doping) is a common method to improve QY. In the Liu et al. research, Poly-γ-glutamic acid (γ-PGA) was utilized as both a carbon and nitrogen source at the same time, and the precursors experienced heating and stirring, pH control, aging, and high-temperature forming Fe_3O_4@CQDs [69]. The QY and magnetism intensity of resulting nanocomposites were 21.6% and 62 emu/g, respectively. The superior characteristics of high QY, good dispersity, excellent colloidal stability, tunable fluorescence, high QY, and strong magnetism make them an advanced probe for triple-modal tumor imaging. In another study, ferric ammonium citrate acted as an iron precursor and carbon source, and triethylenetetramine (TETA) acted as nitrogen source and reducing agent, followed by high-temperature treatment to obtain Fe_3O_4@CQDs in one convenient step [70]. TETA effectively improved the adhesion of CQDs and Fe_3O_4 and gained better crystallinity. The QY of Fe_3O_4@CQDs drastically decreased to 4.6% compared with TETA-CQDs (53%). The static and dynamic fluorescence quenching of CQDs and IFE generated by MNPs conspire to cause this phenomenon. Although the one-pot method provides a rapid, simple, and economic strategy for fabricating bifunctional nanocomposites, the selection of suitable precursors is directly related to the magnetic and fluorescent properties of MNPs@QDs nanocomposites. Impurities are inevitably generated during the reaction period, which affects the separation and purification of products, and cannot achieve precise control of fluorescence and magnetic properties.

Doping transition metal ions or lanthanides into a crystalline lattice of QDs is another strategy for the one-pot preparation of MNPs@QDs. The transition metal ions and lanthanides such as Mn^{2+} [71][72], Eu^{3+} [73], Gd^{3+} [74][75], and Ln^{3+} [76] are used for preparing doped MNPs@QDs. The doped materials are mainly concentrated in biomedical applications and are seldom involved in the rapid detection of food safety. The magnetic intensity of doped materials may be insufficient for the separation and enrichment of complex sample matrix.

References

1. Mahajan, K.D.; Fan, Q.; Dorcena, J.; Ruan, G.; Winter, J.O. Magnetic quantum dots in biotechnology–synthesis and applications. Biotechnol. J. 2013, 8, 1424–1434.
2. Jing, L.; Ding, K.; Kershaw, S.V.; Kempson, I.M.; Rogach, A.L.; Gao, M. Magnetically Engineered Semiconductor Quantum Dots as Multimodal Imaging Probes. Adv. Mater. 2014, 26, 6367–6386.
3. Kim, H.; Achermann, M.; Balet, L.P.; Hollingsworth, J.A.; Klimov, V.I. Synthesis and characterization of Co/CdSe core/shell nanocomposites: Bifunctional magnetic-optical nanocrystals. J. Am. Chem. Soc. 2005, 127, 544–546.

4. Zhou, S.; Chen, Q.; Hu, X.; Zhao, T. Bifunctional luminescent superparamagnetic nanocomposites of CdSe/CdS-Fe3O4 synthesized via a facile method. J. Mater. Chem. 2012, 22, 8263–8270.
5. Bhandari, S.; Khandelia, R.; Pan, U.N.; Chattopadhyay, A. Surface Complexation-Based Biocompatible Magnetofluorescent Nanoprobe for Targeted Cellular Imaging. ACS Appl. Mater. Interfaces 2015, 7, 17552–17557.
6. Wu, Y.; Zou, H.; Zhang, Y.; Mou, M.; Niu, Q.; Yan, Z.; Liao, S. The Loading of Luminescent Magnetic Nanocomposites Fe3O4@Polyaniline/Carbon Dots for Methotrexate and Its Release Behavior In Vitro. J. Nanosci. Nanotechnol. 2020, 20, 701–708.
7. Lee, J.-S.; Bodnarchuk, M.I.; Shevchenko, E.V.; Talapin, D.V. “Magnet-in-the-Semiconductor” FePt-PbS and FePt-PbSe Nanostructures: Magnetic Properties, Charge Transport, and Magnetoresistance. J. Am. Chem. Soc. 2010, 132, 6382–6391.
8. Gu, H.W.; Zheng, R.K.; Zhang, X.X.; Xu, B. Facile one-pot synthesis of bifunctional heterodimers of nanoparticles: A conjugate of quantum dot and magnetic nanoparticles. J. Am. Chem. Soc. 2004, 126, 5664–5665.
9. Selvan, S.T.; Patra, P.K.; Ang, C.Y.; Ying, J.Y. Synthesis of silica-coated semiconductor and magnetic quantum dots and their use in the imaging of live cells. Angew. Chem. Int. Ed. 2007, 46, 2448–2452.
10. Lin, A.W.H.; Ang, C.Y.; Patra, P.K.; Han, Y.; Gu, H.; Le Breton, J.-M.; Juraszek, J.; Chiron, H.; Papaefthymiou, G.C.; Selvan, S.T.; et al. Seed-mediated synthesis, properties and application of gamma-Fe2O3-CdSe magnetic quantum dots. J. Solid State Chem. 2011, 184, 2150–2158.
11. McDaniel, H.; Shim, M. Size and Growth Rate Dependent Structural Diversification of Fe3O4/CdS Anisotropic Nanocrystal Heterostructures. ACS Nano 2009, 3, 434–440.
12. Gao, J.; Zhang, W.; Huang, P.; Zhang, B.; Zhang, X.; Xu, B. Intracellular spatial control of fluorescent magnetic nanoparticles. J. Am. Chem. Soc. 2008, 130, 3710–3711.
13. Du, G.H.; Liu, Z.L.; Lu, Q.H.; Xia, X.; Jia, L.H.; Yao, K.L.; Chu, Q.; Zhang, S.M. Fe3O4/CdSe/ZnS magnetic fluorescent bifunctional nanocomposites. Nanotechnology 2006, 17, 2850–2854.
14. Hines, M.A.; Guyot-Sionnest, P. Synthesis and characterization of strongly luminescing ZnS-Capped CdSe nanocrystals. J. Phys. Chem. 1996, 100, 468–471.
15. Deng, S.; Ruan, G.; Han, N.; Winter, J.O. Interactions in fluorescent-magnetic heterodimer nanocomposites. Nanotechnology 2010, 21, 145605.
16. Beaune, G.; Dubertret, B.; Clement, O.; Vayssettes, C.; Cabuil, V.; Menager, C. Giant vesicles containing magnetic nanoparticles and quantum dots: Feasibility and tracking by fiber confocal fluorescence microscopy. Angew. Chem. Int. Ed. 2007, 46, 5421–5424.

17. Ruan, G.; Vieira, G.; Henighan, T.; Chen, A.; Thakur, D.; Sooryakumar, R.; Winter, J.O. Simultaneous Magnetic Manipulation and Fluorescent Tracking of Multiple Individual Hybrid Nanostructures. Nano Lett. 2010, 10, 2220–2224.
18. Park, J.-H.; von Maltzahn, G.; Ruoslahti, E.; Bhatia, S.N.; Sailor, M.J. Micellar hybrid nanoparticles for simultaneous magnetofluorescent imaging and drug delivery. Angew. Chem. Int. Ed. 2008, 47, 7284–7288.
19. Kim, J.; Lee, J.E.; Lee, J.; Yu, J.H.; Kim, B.C.; An, K.; Hwang, Y.; Shin, C.H.; Park, J.G.; Kim, J.; et al. Magnetic fluorescent delivery vehicle using uniform mesoporous silica spheres embedded with monodisperse magnetic and semiconductor nanocrystals. J. Am. Chem. Soc. 2006, 128, 688–689.
20. Sun, L.; Zang, Y.; Sun, M.D.; Wang, H.G.; Zhu, X.J.; Xu, S.F.; Yang, Q.B.; Li, Y.X.; Shan, Y.M. Synthesis of magnetic and fluorescent multifunctional hollow silica nanocomposites for live cell imaging. J. Colloid Interface Sci. 2010, 350, 90–98.
21. Xiao, Q.; Xiao, C. Preparation and Characterization of Silica-Coated Magnetic-Fluorescent Bifunctional Microspheres. Nanoscale Res. Lett. 2009, 4, 1078–1084.
22. Yi, D.K.; Selvan, S.T.; Lee, S.S.; Papaefthymiou, G.C.; Kundaliya, D.; Ying, J.Y. Silica-coated nanocomposites of magnetic nanoparticles and quantum dots. J. Am. Chem. Soc. 2005, 127, 4990–4991.
23. Ruan, J.; Wang, K.; Song, H.; Xu, X.; Ji, J.J.; Cui, D.X. Biocompatibility of hydrophilic silica-coated CdTe quantum dots and magnetic nanoparticles. Nanoscale Res. Lett. 2011, 6, 13.
24. Kyeong, S.; Jeong, C.; Kim, H.Y.; Hwang, D.W.; Kang, H.; Yang, J.-K.; Lee, D.S.; Jun, B.-H.; Lee, Y.-S. Fabrication of mono-dispersed silica-coated quantum dot-assembled magnetic nanoparticles. RSC Adv. 2015, 5, 32072–32077.
25. Huang, L.; Zhang, Y.; Liao, T.; Xu, K.; Jiang, C.; Zhuo, D.; Wang, Y.; Wen, H.-M.; Wang, J.; Ao, L.; et al. Compact Magneto-Fluorescent Colloids by Hierarchical Assembly of Dual-Components in Radial Channels for Sensitive Point-of-Care Immunoassay. Small 2021, 17, 2100862.
26. Tan, Y.F.; Chandrasekharan, P.; Maity, D.; Yong, C.X.; Chuang, K.-H.; Zhao, Y.; Wang, S.; Ding, J.; Feng, S.-S. Multimodal tumor imaging by iron oxides and quantum dots formulated in poly (lactic acid)-D-alpha-tocopheryl polyethylene glycol 1000 succinate nanoparticles. Biomaterials 2011, 32, 2969–2978.
27. Xie, H.Y.; Zuo, C.; Liu, Y.; Zhang, Z.L.; Pang, D.W.; Li, X.L.; Gong, J.P.; Dickinson, C.; Zhou, W.Z. Cell-targeting multifunctional nanospheres with both fluorescence and magnetism. Small 2005, 1, 506–509.
28. Li, Y.-H.; Song, T.; Liu, J.-Q.; Zhu, S.-J.; Chang, J. An efficient method for preparing high-performance multifunctional polymer beads simultaneously incorporated with magnetic

nanoparticles and quantum dots. J. Mater. Chem. 2011, 21, 12520–12528.

29. Wilson, R.; Spiller, D.G.; Prior, I.A.; Veltkamp, K.J.; Hutchinson, A. A Simple Method for Preparing Spectrally Encoded Magnetic Beads for Multiplexed Detection. ACS Nano 2007, 1, 487–493.
30. Wang, C.; Wang, L.; Yang, W. Preparation and characterization of functional inorganic/organic composite microspheres via electrostatic interaction. J. Colloid Interface Sci. 2009, 333, 749–756.
31. Li, L.; Choo, E.S.G.; Liu, Z.; Ding, J.; Xue, J. Double-layer silica core-shell nanospheres with superparamagnetic and fluorescent functionalities. Chem. Phys. Lett. 2008, 461, 114–117.
32. Yin, N.; Wang, X.; Yang, T.; Ding, Y.; Li, L.; Zhao, S.; Li, P.; Xu, X.; Zhu, L. Multifunctional Fe3O4 quantum dot-embedded mesoporous SiO2 nanoplatform probe for cancer cell fluorescence-labelling detection and photothermal therapy. Ceram. Int. 2021, 47, 8271–8278.
33. Yoo, J.H.; Kim, J.S. The Preparation of Core-Shell Magnetic Silica Nanospheres for Enhancing Magnetism and Fluorescence Intensity. J. Nanosci. Nanotechnol. 2013, 13, 7615–7619.
34. Sathe, T.R.; Agrawal, A.; Nie, S. Mesoporous silica beads embedded with semiconductor quantum dots and iron oxide nanocrystals: Dual-function microcarriers for optical encoding and magnetic separation. Anal. Chem. 2006, 78, 5627–5632.
35. Xie, H.-Y.; Xie, M.; Zhang, Z.-L.; Long, Y.-M.; Liu, X.; Tang, M.-L.; Pang, D.-W.; Tan, Z.; Dickinson, C.; Zhou, W. Wheat germ agglutinin-modified trifunctional nanospheres for cell recognition. Bioconjugate Chem. 2007, 18, 1749–1755.
36. Zebli, B.; Susha, A.S.; Sukhorukov, G.B.; Rogach, A.L.; Parak, W.J. Magnetic Targeting and Cellular Uptake of Polymer Microcapsules Simultaneously Functionalized with Magnetic and Luminescent Nanocrystals. Langmuir 2005, 21, 4262–4265.
37. Li, Z.; Wang, G.; Shen, Y.; Guo, N.; Ma, N. DNA-Templated Magnetic Nanoparticle-Quantum Dot Polymers for Ultrasensitive Capture and Detection of Circulating Tumor Cells. Adv. Funct. Mater. 2018, 28, 1707152.
38. Zou, W.-S.; Yang, J.; Yang, T.-T.; Hu, X.; Lian, H.-Z. Magnetic-room temperature phosphorescent multifunctional nanocomposites as chemosensor for detection and photo-driven enzyme mimetics for degradation of 2,4,6-trinitrotoluene. J. Mater. Chem. 2012, 22, 4720–4727.
39. Ortgies, D.H.; de la Cueva, L.; del Rosal, B.; Sanz-Rodríguez, F.; Fernández, N.; Iglesias-de la Cruz, M.C.; Salas, G.; Cabrera, D.; Teran, F.J.; Jaque, D.; et al. In Vivo Deep Tissue Fluorescence and Magnetic Imaging Employing Hybrid Nanostructures. ACS Appl. Mater. Interfaces 2016, 8, 1406–1414.
40. Xiao, L.-H.; Wang, T.; Zhao, T.-Y.; Zheng, X.; Sun, L.-Y.; Li, P.; Liu, F.-Q.; Gao, G.; Dong, A. Fabrication of Magnetic-Antimicrobial-Fluorescent Multifunctional Hybrid Microspheres and Their Properties. Int. J. Mol. Sci. 2013, 14, 7391–7404.

41. Fan, H.-M.; Olivo, M.; Shuter, B.; Yi, J.-B.; Bhuvaneswari, R.; Tan, H.-R.; Xing, G.-C.; Ng, C.-T.; Liu, L.; Lucky, S.S.; et al. Quantum Dot Capped Magnetite Nanorings as High Performance Nanoprobe for Multiphoton Fluorescence and Magnetic Resonance Imaging. J. Am. Chem. Soc. 2010, 132, 14803–14811.
42. Hong, X.; Li, J.; Wang, M.J.; Xu, J.J.; Guo, W.; Li, J.H.; Bai, Y.B.; Li, T.J. Fabrication of magnetic luminescent nanocomposites by a layer-by-layer self-assembly approach. Chem. Mater. 2004, 16, 4022–4027.
43. Wang, C.W.; Shen, W.Z.; Rong, Z.; Liu, X.X.; Gu, B.; Xiao, R.; Wang, S.Q. Layer-by-layer assembly of magnetic-core dual quantum dot-shell nanocomposites for fluorescence lateral flow detection of bacteria. Nanoscale 2020, 12, 795–807.
44. Chen, B.; Zhang, H.; Zhai, C.; Du, N.; Sun, C.; Xue, J.; Yang, D.; Huang, H.; Zhang, B.; Xie, Q.; et al. Carbon nanotube-based magnetic-fluorescent nanohybrids as highly efficient contrast agents for multimodal cellular imaging. J. Mater. Chem. 2010, 20, 9895–9902.
45. Sun, X.; Ding, K.; Hou, Y.; Gao, Z.; Yang, W.; Jing, L.; Gao, M. Bifunctional Superparticles Achieved by Assembling Fluorescent CuInS2@ZnS Quantum Dots and Amphibious Fe3O4 Nanocrystals. J. Phys. Chem. C 2013, 117, 21014–21020.
46. Wang, D.; He, J.; Rosenzweig, N.; Rosenzweig, Z. Superparamagnetic Fe2O3 Beads−CdSe/ZnS Quantum Dots Core−Shell Nanocomposite Particles for Cell Separation. Nano Lett. 2004, 4, 409–413.
47. Nikitin, M.P.; Zdobnova, T.A.; Lukash, S.V.; Stremovskiy, O.A.; Deyev, S.M. Protein-assisted self-assembly of multifunctional nanoparticles. Proc. Natl. Acad. Sci. USA 2010, 107, 5827.
48. Shibu, E.S.; Ono, K.; Sugino, S.; Nishioka, A.; Yasuda, A.; Shigeri, Y.; Wakida, S.-i.; Sawada, M.; Biju, V. Photouncaging Nanoparticles for MRI and Fluorescence Imaging in Vitro and in Vivo. ACS Nano 2013, 7, 9851–9859.
49. Song, E.; Han, W.; Xu, H.; Jiang, Y.; Cheng, D.; Song, Y.; Swihart, M.T. Magnetically Encoded Luminescent Composite Nanoparticles through Layer-by-Layer Self-Assembly. Chem.—Eur. J. 2014, 20, 14642–14649.
50. Rong, Z.; Bai, Z.K.; Li, J.N.; Tang, H.; Shen, T.Y.; Wang, Q.; Wang, C.W.; Xiao, R.; Wang, S.Q. Dual-color magnetic-quantum dot nanobeads as versatile fluorescent probes in test strip for simultaneous point-of-care detection of free and complexed prostate-specific antigen. Biosens. Bioelectron. 2019, 145, 8.
51. Wang, C.; Cheng, X.; Liu, L.; Zhang, X.; Yang, X.; Zheng, S.; Rong, Z.; Wang, S. Ultrasensitive and Simultaneous Detection of Two Specific SARS-CoV-2 Antigens in Human Specimens Using Direct/Enrichment Dual-Mode Fluorescence Lateral Flow Immunoassay. ACS Appl. Mater. Interfaces 2021, 13, 40342–40353.

52. Dong, S.; Wang, S.; Wang, X.; Zhai, L. Superparamagnetic nanocomposite Fe3O4@SiO2-NH2/CQDs as fluorescent probe for copper (II) detection. Mater. Lett. 2020, 278, 128404.
53. Zhang, X.; Tang, B.; Li, Y.; Liu, C.; Jiao, P.; Wei, Y. Molecularly Imprinted Magnetic Fluorescent Nanocomposite-Based Sensor for Selective Detection of Lysozyme. Nanomaterials 2021, 11, 1575.
54. Li, C.-L.; Huang, B.-R.; Chang, J.-Y.; Chen, J.-K. Bifunctional superparamagnetic-luminescent core-shell-satellite structured microspheres: Preparation, characterization, and magnetodisplay application. J. Mater. Chem. C 2015, 3, 4603–4615.
55. Koc, K.; Karakus, B.; Rajar, K.; Alveroglu, E. Synthesis and characterization. of 3O4 fluorescent-magnetic bifunctional nanospheres. Superlattices Microstruct. 2017, 110, 198–204.
56. Wang, K.; Xu, X.; Li, Y.; Rong, M.; Wang, L.; Lu, L.; Wang, J.; Zhao, F.; Sun, B.; Jiang, Y. Preparation Fe3O4@chitosan-graphene quantum dots nanocomposites for fluorescence and magnetic resonance imaging. Chem. Phys. Lett. 2021, 783, 139060.
57. Wang, Z.; Jiang, X.; Liu, W.; Lu, G.; Huang, X. A rapid and operator-safe powder approach for latent fingerprint detection using hydrophilic Fe3O4@SiO2-CdTe nanoparticles. Sci. China Chem. 2019, 62, 889–896.
58. Wang, M.; Fei, X.F.; Lv, S.W.; Sheng, Y.; Zou, H.F.; Song, Y.H.; Yan, F.; Zhu, Q.L.; Zheng, K.Y. Synthesis and characterization of a flexible fluorescent magnetic Fe3O4@SiO2/CdTe-NH2 nanoprobe. J. Inorg. Biochem. 2018, 186, 307–316.
59. Zhang, Y.; Wang, S.-N.; Ma, S.; Guan, J.-J.; Li, D.; Zhang, X.-D.; Zhang, Z.-D. Self-assembly multifunctional nanocomposites with Fe3O4 magnetic core and CdSe/ZnS quantum dots shell. J. Biomed. Mater. Res. Part A 2008, 85A, 840–846.
60. Chen, O.; Riedemann, L.; Etoc, F.; Herrmann, H.; Coppey, M.; Barch, M.; Farrar, C.T.; Zhao, J.; Bruns, O.T.; Wei, H.; et al. Magneto-fluorescent core-shell supernanoparticles. Nat. Commun. 2014, 5, 5093.
61. Piao, Y.; Burns, A.; Kim, J.; Wiesner, U.; Hyeon, T. Designed Fabrication of Silica-Based Nanostructured Particle Systems for Nanomedicine Applications. Adv. Funct. Mater. 2008, 18, 3745–3758.
62. Guo, L.; Shao, Y.; Duan, H.; Ma, W.; Leng, Y.; Huang, X.; Xiong, Y. Magnetic Quantum Dot Nanobead-Based Fluorescent Immunochromatographic Assay for the Highly Sensitive Detection of Aflatoxin B1 in Dark Soy Sauce. Anal. Chem. 2019, 91, 4727–4734.
63. Guo, S.; Chen, Y.-Q.; Lu, N.-N.; Wang, X.-Y.; Xie, M.; Sui, W.-P. Ultrasonication-assisted one-step self-assembly preparation of biocompatible fluorescent-magnetic nanobeads for rare cancer cell detection. Nanotechnology 2014, 25, 505603.

64. Kim, J.; Lee, J.E.; Lee, S.H.; Yu, J.H.; Lee, J.H.; Park, T.G.; Hyeon, T. Designed fabrication of a multifunctional polymer nanomedical platform for simultaneous cancer-targeted imaging and magnetically guided drug delivery. Adv. Mater. 2008, 20, 478–483.

65. Leng, Y.; Wu, W.; Li, L.; Lin, K.; Sun, K.; Chen, X.; Li, W. Magnetic/Fluorescent Barcodes Based on Cadmium-Free Near-Infrared-Emitting Quantum Dots for Multiplexed Detection. Adv. Funct. Mater. 2016, 26, 7581–7589.

66. Lan, J.; Chen, J.; Li, N.; Ji, X.; Yu, M.; He, Z. Microfluidic generation of magnetic-fluorescent Janus microparticles for biomolecular detection. Talanta 2016, 151, 126–131.

67. Zhou, C.; Wang, Z.; Xia, J.; Via, B.K.; Zhang, F.; Xia, Y.; Li, Y. A simplistic one-pot method to produce magnetic graphene-CdS nanocomposites. Comptes Rendus Chim. 2012, 15, 714–718.

68. Maleki, S.; Madrakian, T.; Afkhami, A. Magnetic solid-phase extraction of codeine in a biological sample utilizing Fe3O4/CDs/Lys nanocomposite as an efficient adsorbent. J. Iran. Chem. Soc. 2019, 16, 2111–2121.

69. Liu, X.; Jiang, H.; Ye, J.; Zhao, C.; Gao, S.; Wu, C.; Li, C.; Li, J.; Wang, X. Nitrogen-Doped Carbon Quantum Dot Stabilized Magnetic Iron Oxide Nanoprobe for Fluorescence, Magnetic Resonance, and Computed Tomography Triple-Modal In Vivo Bioimaging. Adv. Funct. Mater. 2016, 26, 8694–8706.

70. Li, B.; Wang, X.; Guo, Y.; Iqbal, A.; Dong, Y.; Li, W.; Liu, W.; Qin, W.; Chen, S.; Zhou, X.; et al. One-pot synthesis of polyamines improved magnetism and fluorescence Fe3O4-carbon dots hybrid NPs for dual modal imaging. Dalton Trans. 2016, 45, 5484–5491.

71. Irmania, N.; Dehvari, K.; Gedda, G.; Tseng, P.-J.; Chang, J.-Y. Manganese-doped green tea-derived carbon quantum dots as a targeted dual imaging and photodynamic therapy platform. J. Biomed. Mater. Res. Part B 2020, 108, 1616–1625.

72. Ji, Z.; Ai, P.; Shao, C.; Wang, T.; Yan, C.; Ye, L.; Gu, W. Manganese-Doped Carbon Dots for Magnetic Resonance/Optical Dual-Modal Imaging of Tiny Brain Glioma. ACS Biomater. Sci. Eng. 2018, 4, 2089–2094.

73. Yao, Y.-Y.; Gedda, G.; Girma, W.M.; Yen, C.-L.; Ling, Y.-C.; Chang, J.-Y. Magnetofluorescent Carbon Dots Derived from Crab Shell for Targeted Dual-Modality Bioimaging and Drug Delivery. ACS Appl. Mater. Interfaces 2017, 9, 13887–13899.

74. Liao, H.; Wang, Z.; Chen, S.; Wu, H.; Ma, X.; Tan, M. One-pot synthesis of gadolinium(III) doped carbon dots for fluorescence/magnetic resonance bimodal imaging. RSC Adv. 2015, 5, 66575–66581.

75. Yu, C.; Xuan, T.; Chen, Y.; Zhao, Z.; Liu, X.; Lian, G.; Li, H. Gadolinium-doped carbon dots with high quantum yield as an effective fluorescence and magnetic resonance bimodal imaging probe. J. Alloys Compd. 2016, 688, 611–619.

76. Wu, F.; Yue, L.; Yang, L.; Wang, K.; Liu, G.; Luo, X.; Zhu, X. Ln(III) chelates-functionalized carbon quantum dots: Synthesis, optical studies and multimodal bioimaging applications. Colloids Surf. B 2019, 175, 272–280.